First-principles study of uranium carbide: Accommodation of point defects and of helium, xenon, and oxygen impurities

Michel Freyss*
CEA, DEN, Centre de Cadarache, DEC/SESC/LLCC, F-13108 Saint-Paul-lez-Durance, France
(Received 21 August 2009; revised manuscript received 23 November 2009; published 4 January 2010)

Point defects and volatile impurities (helium, xenon, oxygen) in uranium monocarbide UC are studied by first-principles calculations. Preliminarily, bulk properties of UC and of two other uranium carbide phases, UC_2 and U_2C_3, are calculated in order to compare them to experimental data and to get confidence in the use of the generalized gradient approximation for this class of compounds. The subsequent study of different types of point defects shows that the carbon sublattice best accommodates the defects. The perturbation of the crystal structure induced by the defects is weak and the interaction between defects is found short range. Interstitial carbon dumbbells possibly play an important role in the diffusion of carbon atoms. The most favorable location of diluted helium, xenon, and oxygen impurities in the UC crystal lattice is then determined. The rare-gas atoms occupy preferably a uranium substitution site or a uranium site in a U-C bivacancy. But their incorporation in UC is, however, not energetically favorable, especially for xenon, suggesting their propensity to diffuse in the material and/or form bubbles. On the other hand, oxygen atoms are very favorably incorporated as diluted atoms in the UC lattice, confirming the easy oxidation of UC. The oxygen atoms preferably occupy a carbon substitution site or the carbon site of a U-C bivacancy. Our results are compared to available experimental data on UC and to similar studies by first-principles calculations for other carbides and nitrides with the rock-salt structure.

DOI: 10.1103/PhysRevB.81.014101 PACS number(s): 61.72.J−, 61.72.S−, 71.15.Mb

I. INTRODUCTION

Mixed uranium-plutonium carbides are widely studied materials for their potential applications as nuclear fuels in so-called Generation IV reactors.[1,2] These compounds present several advantages compared to standard oxide fuels: a higher actinide density, a higher fusion temperature and a greater thermal conductivity, among others. In the case of uranium carbides, the monocarbide UC is stable in a large domain of compositions in its rock-salt structure (UC_x with $0.95 < x < 2.00$ at high temperature) because of its solubility with the tetragonal UC_2 phase.[3]

The aim of this paper is to shed light on irradiation damage in uranium monocarbide UC, as a first step in the study of the mixed uranium-plutonium carbides. On the one hand, the stability of point defects is studied: the knowledge of the type of defects which can be created and the assessment of their formation energies is of prime importance to get some insight into the behavior at the atom scale of the material under irradiation. Those data give information on how the material accommodates irradiation damage and deviation from stoichiometry. Point defects, such as vacancies or vacancy clusters, can also constitute traps for impurities and fission products. Point defects of the following types are considered here: interstitials, vacancies, bivacancies, dumbbells, Frenkel pairs, and antisite defects.

On the second hand, the stability in UC of impurities such as helium, xenon, and oxygen atoms is studied. Impurities can significantly modify the properties of the material, which is also a key issue for applications as a nuclear fuel. Helium atoms appear in the compound as a result of α decays, xenon is one of the fission product produced in the largest amount and oxygen can be incorporated in the material by oxidation. For each of these elements, the most favorable incorporation site in the UC lattice is determined. Their stability in the lattice also enables us to assess their solubility in the compound.

For this study of point defects and of impurities in UC, the first-principles projector augmented wave (PAW) method,[4,5] based on the density-functional theory (DFT),[6,7] is used. The plane-wave expansion of the electron basis is particularly adequate to relax the atomic positions around the defects and the impurities. The generalized gradient approximation (GGA) is used for the exchange-correlation interaction. As will be shown, a preliminary study of some bulk properties of UC indicates that the GGA gives satisfactory results compared to experimental data. An approximation beyond LDA/GGA does not appear to be required for UC, as it is the case for other uranium compounds such as UO_2 (Refs. 8–12) for which the localization and the correlations of the $5f$ electrons are stronger. The GGA approximation also proved to give good results for metallic α uranium[13,14] as well as uranium nitride.[15,16] It is to be stressed that calculations using approximations beyond LDA and GGA such as the DFT+U approximation are much more time-consuming and are complicated by the existence of local energy minima.[12] Furthermore, using the self-interaction corrected local spin-density (SIC-LSD) method, Petit *et al.*[17] confirmed that the treatment of the $5f$ electrons of UC as delocalized, like assumed by GGA calculations, is indeed adequate. It is also to be noted that although the DFT is known to poorly describe van der Waals interactions, which are of importance in the binding properties of rare-gas atoms such as helium and xenon studied here, it is assumed in this paper that DFT GGA will anyhow give reliable trends for the incorporation of such diluted impurities, as it has already been shown for helium atoms in iron, for instance.[18] Nonlocal van der Waals density functionals are being developed[19,20] but

they are not yet available in plane-wave codes.

To our knowledge, besides first-principles studies of bulk properties of UC (Refs. 17 and 21–26) in which the Xα, the LDA/GGA, or the SIC-LSD approximations were used, no first-principles study of point defects and of impurities in UC exist. Furthermore, few experimental data are available. Bowman *et al.*[27] and Sarian[28] could identify experimentally some defects in UC. Values for the formation energies of point defects were proposed by Matzke,[29] Donner and Schüle,[30] Schüle and Spindler,[31] Griffiths[32] and Matsui *et al.*[33,34] These values are also discussed in a review by Matzke.[35] The disparity or the lack of experimental values for the formation energies of some point defects are the main motivations for the present *ab initio* study. The results obtained will also be compared to experimental and theoretical studies of some other carbides, nitrides, or oxides exhibiting a rock-salt structure: UN,[16,36–39] ZrC,[40] TiC,[41] MgO,[42,43] TiN, ZrN, and HfN.[44,45]

This study also constitutes a first step toward the calculations of atomic transport properties in UC, in particular the determination of the migration mechanisms of uranium and carbon atoms or of impurities in the crystal lattice. Such calculations will make a direct link to calculation techniques at larger scales, which require accurate experimental or theoretical data for the adjustment of empirical parameters, such as those used in classical molecular dynamics,[46] kinetic Monte Carlo simulations or diffusion models.

The paper is organized as follows. In the Sec. II, the first-principles method of calculation used is briefly presented, together with the approximations made. In the Sec. III, the bulk properties of UC calculated in the GGA approximation are reported and compared to experimental data. Results on the bulk UC_2 and U_2C_3 phases are also given. In the Sec. IV, the calculated formation energies of point defects are reported, together with an analysis of the perturbation these defects induce on the lattice structure and the charge density. The interaction between single defects is also discussed. Finally, in the Sec. V, the results on the incorporation of helium, xenon, and oxygen impurities in UC are reported.

II. METHOD OF CALCULATION

The first-principles PAW method[4,5] as implemented in the code VASP (Refs. 47 and 48) is used. The exchange-correlation interaction is taken into account in the GGA as parametrized by Perdew-Burke-Ernzerhof (PBE).[49] Fourteen electrons ($6s^26p^65f^36d^17s^2$) for uranium and four electrons ($2s^22p^2$) for carbon are taken into account as valence electrons, and the core electron density is frozen. Some basic bulk properties of UC calculated with this PAW method will be subsequently compared to results obtained with the all-electron APW+lo (augmented plane waves and local orbitals) method to show that this limitation has no influence on the accuracy of the results presented here. A 350 eV cut-off energy for the plane-wave expansion of the electron basis is chosen and a $4\times4\times4$ Monkhorst-Pack k-point mesh[50] is used to sample the Brillouin zone of the 64-atom supercell for the modeling of the point defects and impurities in UC. Such a sampling and expansion are enough to get the energy differences required in the calculation of the defect-formation energies and the impurity incorporation energies converged to less than 30 meV. In all calculations of the stability of the point defects and impurities, the atomic positions are relaxed until the maximum forces are less than 10^{-4} eV/Å. Volume relaxation of the supercell is also taken into account. Spin polarization is not taken into account. As it will be shown later, UC is found to display a small magnetic moment. The neglect of the spin polarization was tested in the calculation of the formation energy of a U-C bivacancy and lead to a difference of less than 40 meV.

TABLE I. Lattice parameter a (Å) and bulk modulus (GPa) of UC and UO_2 calculated with the PAW and the APW+lo methods, and comparison to experimental data (Refs. 53–55).

	PAW	APW+lo	Experimental
UC	a=4.93 Å	a=4.94 Å	a=4.96 Å
	B=185 GPa	B=183 GPa	B=167 GPa
UO_2	a=5.39 Å	a=5.38 Å	a=5.47 Å
	B=204 GPa	B=205 GPa	B=207 GPa

III. RESULTS ON PROPERTIES OF BULK URANIUM CARBIDES

Results are reported here on calculated bulk properties of uranium carbides UC, UC_2, and U_2C_3 obtained with the GGA approximation. We focus on the structure, the bulk modulus and the magnetic properties, and compare the formation energies of the three bulk compounds. As a first step, some bulk properties of the monocarbide UC calculated with the PAW method are compared with those calculated with the more accurate all-electron first-principles APW+lo method[51] as implemented in the code WIEN2K.[52] For both methods the same GGA-PBE functional[49] is used and the spin polarization is neglected. This comparison is a way of testing the PAW atomic data for U and C used as input quantities and which are provided with the code VASP. The APW+lo method does not require such atomic data since the electron core states are explicitly calculated. It is thus a more accurate method but APW+lo calculations become much more time consuming when the number of atoms increases. This justifies that the studies on defect and impurity stability be rather performed using the PAW method.

A. Comparison of the PAW and APW+lo methods for bulk UC

The comparison for the lattice parameter and the bulk modulus of UC calculated using both methods are reported in Table I. The comparison for the same properties of UO_2 is also added. The UC crystal is modeled in its rock-salt NaCl structure with two atoms per unit cell and the UO_2 crystal in its fluorite structure with three atoms, not taking into account the spin polarization. In the APW+lo calculations, the basis set is expanded with the parameter $RK_{max}=7$ and the irreducible Brillouin zone is sampled by 72 k points.

For both UC and UO_2 the PAW method gives results very close to those obtained with the APW+lo method. The PAW atomic data for each chemical element, in particular uranium, are thus very satisfactory.

By comparison with the experimental data for UC,[54] the structural properties are very well described by the nonspin-polarized (NSP) GGA calculations, with less than 1% error on the lattice parameter. On the other hand, the NSP-GGA approximation yields a bulk modulus which appears 11% too large compared to the experimental value: 185 GPa by the PAW calculation against 167 GPa experimentally.[53] It will be shown later that taking into account the spin polarization does not modify much the calculated value of the bulk modulus and thus does not improve the agreement between the calculated and experimental values. A possible explanation for the discrepancy could be the nonstoichiometry of UC. The influence of carbon vacancies on the bulk modulus will be investigated subsequently, in order to check whether the GGA calculations can reproduce the experimental behavior of the bulk modulus with the deviation of stoichiometry of UC.

It is also to be stressed that the calculations are made here in the scalar-relativistic approximation. The influence of the spin-orbit coupling has not yet been investigated for UC. It has, however, already been shown by Sedmidubsky *et al.*[36] that the spin-orbit coupling had little effect (of only around 50 meV/f.u.) on the calculated enthalpies of formation and cohesive energies of actinide nitrides. Moreover, the GGA calculations by Atta-Fynn and Ray[15] showed that, for actinide nitrides as well, a variation of ± 10 GPa of the bulk modulus can be obtained when taking into account the spin-orbit coupling. One could expect a similar trend for uranium carbide.

B. Bulk modulus of nonstoichiometric UC

As stressed in the previous section, the calculated value of the bulk modulus of UC is overestimated by 11% compared to the experimental value. We check here that the calculated bulk modulus nonetheless follows the experimental behavior as a function of the deviation from stoichiometry of the compound. The effect of a slight deviation from stoichiometry is investigated by calculating the bulk modulus in hyposto-ichiometric UC, i.e., containing vacancies in the carbon sublattice. The compounds $UC_{0.969}$ and $UC_{0.938}$ are modeled introducing one or two carbon vacancies, respectively, in a 64-atom UC supercell. When two vacancies are considered in the same supercell (for $UC_{0.938}$), the largest distance possible separating the two vacancies is chosen. In such a configuration the interaction between both defects is negligible since the interaction range between defects in UC does not exceed the second-nearest-neighbor distance (4.93 Å), as it will be shown in the subsequent section on point defects.

The calculated values for the bulk modulus of UC, $UC_{0.969}$, and $UC_{0.938}$ are 185, 176, and 170 GPa, respectively. Taking into account carbon vacancies thus reduces the bulk modulus of the compound of 10 GPa for $UC_{0.969}$ and of 15 GPa for $UC_{0.938}$ compared to stoichiometric UC. Figure 1 represents the variation in the bulk modulus with the deviation x from stoichiometry of UC_x as calculated and as measured experimentally on UC single crystals.[53] The calculated values follow well the experimental behavior, with a constant overestimation of the calculated values.

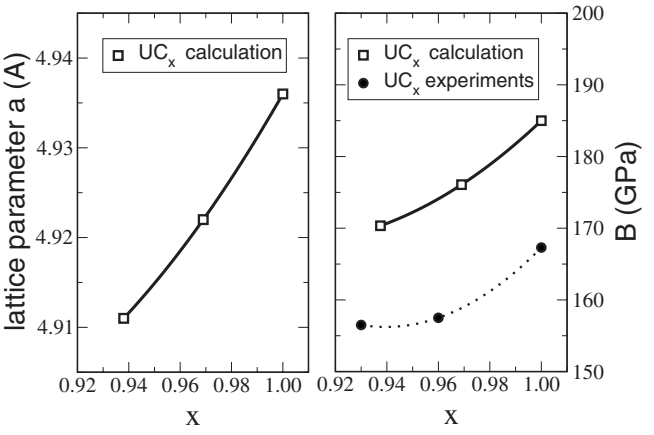

FIG. 1. Lattice parameter (left) and bulk modulus (right) as a function of the deviation from stoichiometry x in UC_x, calculated in a 64-atom supercell containing two carbon vacancies ($UC_{0.9375}$), one carbon vacancy ($UC_{0.969}$), or no defect (UC).

The lattice parameters obtained for $UC_{0.969}$ and $UC_{0.938}$ are also shown on Fig. 1. They are not so different from the one of the stoichiometric compound: 4.92 Å for $UC_{0.969}$, that is hardly 0.3 % smaller than that of UC, and of 4.91 Å for $UC_{0.938}$, that is 0.4 % smaller.

Thus, even if the GGA calculation does not reproduce exactly the experimental value of the bulk modulus, it has been shown here that it could at least reproduce its behavior as a function of stoichiometry in hypostoichiometric UC. The error of around 10% on the value of the bulk modulus of stoichiometric UC can nonetheless be considered acceptable in regard to DFT studies of solids in general.

C. Magnetic properties of UC

In this section, the magnetic properties of UC are investigated. The relative stability of three different magnetic orders is calculated: a ferromagnetic (FM) order and two-layered antiferromagnetic orders (AFM-I and AFM-II), whose stabilities are compared to the nonmagnetic (NM) configuration. In the type-I layered antiferromagnetic order (AFM-I), the uranium magnetic moments in a (100) layer point in the same direction and opposite to the moments of the next (100) atomic layer. Similarly, the type-II-layered antiferromagnetic order (AFM-II) is constituted by an alternation of (111) layer with opposite uranium magnetic moments. Experimentally UC is supposed to behave like a Pauli paramagnet.[56] In Table II are reported some calculated bulk properties (equilibrium lattice parameter, bulk modulus, and magnetic moment) of UC in the magnetic configurations considered and the relative energies of these configurations.

The AFM-I state is found the most stable magnetic state, with only a slight energy difference of 0.1 meV/f.u. compared to the nonmagnetic state. Neither the FM order nor the AFM-II order was actually obtained at their equilibrium lattice parameter: these states converge to the nonmagnetic

TABLE II. Lattice parameter a (in Å), bulk modulus B (in GPa), uranium magnetic moment m (in μ_B/U atom), and relative stability ΔE (in meV/UC) calculated in the nonmagnetic (NM) and type-I antiferromagnetic (AFM-I) configurations, and comparison to experimental data (Refs. 53 and 54).

	a (Å)	B (GPa)	m (μ_B)	ΔE (meV)
NM	4.931	185	0	0
AFM-I	4.936	182	± 0.2	−0.12
Expt.	4.960	167		

state when relaxing the lattice parameter. At equilibrium, only the antiferromagnetic AFM-I configuration yields finite values for the magnetic moments, which are, moreover, very small. They amount to only $\pm 0.2\mu_B$ and are carried by the uranium atoms and their $5f$ electrons. For comparison, similar calculations for UN and UO_2 with the same PAW-GGA approach yield values of ± 1.1 and $\pm 1.4\mu_B$, respectively, for the uranium AFM-I moments. It should also be stressed that an insufficient sampling of the Brillouin zone lead to a wrong ground-state magnetic order. With a Monkhorst-Pack mesh smaller than $8\times 8\times 8$ for an eight-atom cubic supercell (or smaller than $4\times 4\times 4$ for the 64-atom cubic supercell), the ferromagnetic configuration is the ground state at the equilibrium lattice parameter.

The calculations here furthermore show that UC is just at the edge of magnetism. According to Hill's criterion,[57] there exists a critical distance between the U atoms (of 3.5 Å) above which the overlap of the $5f$ orbital becomes negligible and magnetism can appear. The equilibrium lattice parameter of UC corresponds to a uranium-uranium distance very close to Hill's critical distance, as it can be seen in Fig. 2. In this figure, are represented, the calculated uranium magnetic moment as a function of the lattice parameter of UC in the three magnetic orders considered (FM, AFM-I, and AFM-II). The calculated equilibrium lattice parameter is represented by the vertical black line, and the lattice parameter corresponding to Hill's distance by the gray line. It is also clearly visible from Fig. 2 that UC displays a weak magnetic moment ($\pm 0.2\mu_B$) at the equilibrium lattice parameter and that a contraction of only 0.8% of this lattice parameter is enough to make the magnetic moment vanish. The FM and the AFM-II magnetic orders only appear for lattice parameters larger than the equilibrium one, 4.94 and 5.08 Å, respectively.

Although the magnetic moment of uranium is small in UC, the effect of the magnetic order could be significant in the calculation of the formation energies of point defects. The change in coordination number and in interatomic distances induced by a defect could enhance or reduce the magnetic moments, as it is also suggested by Fig. 2. Two test calculations were carried out to show that this effect in UC is only very small. Taking into account the AFM-I order, the calculated formation energy of a U-C bivacancy and the incorporation energy of an interstitial helium atom differed by less than 40 meV compared to the same calculations in a nonmagnetic compound. And this in spite of the enhancement of the uranium magnetic moments from 0.2 to $0.6\mu_B$ in the vicinity of the bivacancy. These results thus justify the neglect of the spin polarization in the calculations on the stability of point defects and impurities in UC reported in the following sections.

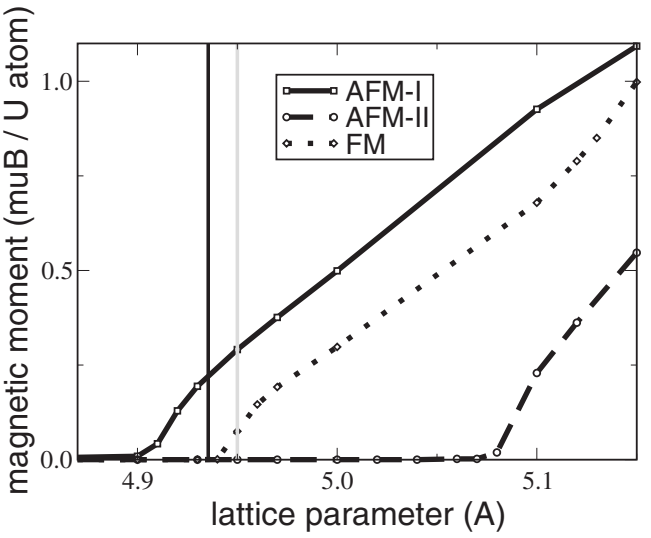

FIG. 2. Calculated variation in the uranium magnetic moment in UC in three different magnetic configurations (AFM-I, AFM-II, and FM) as a function of the lattice parameter. Vertical black line: calculated equilibrium lattice parameter. Vertical gray line: lattice parameter corresponding to Hill's critical distance (see text). The calculations were performed in a 64-atom supercell required to model the AFM-II order.

D. Electron density of states

The atom and orbital projected densities of states (DOSs) of bulk UC are shown in Fig. 3. The DOS were calculated in a four-atom cell displaying the type-I antiferromagnetic order. Spin-up and spin-down DOS have identical features with a small $5f$ electron splitting corresponding to the small ura-

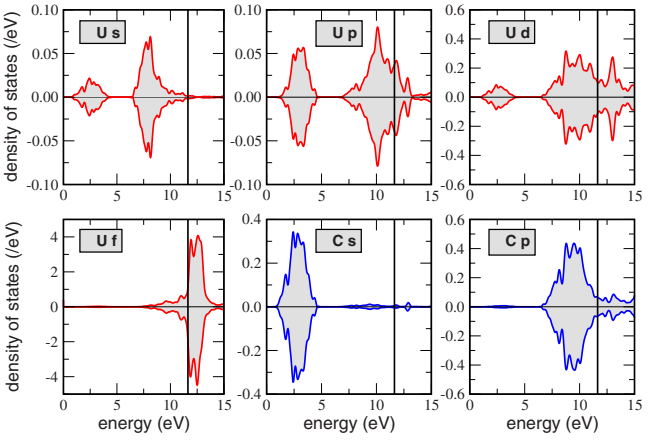

FIG. 3. (Color online) Electron density of states of UC, projected for each atom (uranium and carbon) and each orbital (s, p, d, and f). For more clarity, the vertical scales are varied for each graph. Positive and negative densities of state correspond to spin-up and spin-down states, respectively, and the vertical line to the Fermi level.

TABLE III. Structural properties calculated for α-UC_2, β-UC_2, and U_2C_3, and comparison to experimental data (Refs. 54 and 64–67).

U-C		a (Å)	c/a	z	x_1	x_2
α-UC_2	Calc.	3.517	1.696	0.384		
	Expt.[b]	3.522	1.700	0.389		
	Expt.[c]	3.519	1.699			
	Expt.[a]	3.509	1.704	0.388		
β-UC_2	Calc.	5.389				
	Expt.[d]	5.41				
U_2C_3	Calc.	8.031			0.0490	0.2852
	Expt.[e]	8.089			0.0485	0.2872
	Expt.[a]	8.0885			0.050	0.295

[a]Reference 54.
[b]Reference 64.
[c]Reference 65.
[d]Reference 66.
[e]Reference 67.

nium magnetic moment. Figure 3 shows that UC is metallic with a narrow $5f$ electron peak at the Fermi level. One also notices the strong U-f and C-p hybridization. The hybridization is also revealed by the large charge transfer between C and U atoms. The analysis of the charge density by a Bader decomposition[58] shows that the charge transfer amounts to 1.6 electrons from U atoms toward C atoms, relative to the atomic occupations. Such a charge transfer is obtained in both antiferromagnetic and nonmagnetic UC, showing again that the influence of the spin polarization is not significant on the calculated electronic properties of the compound. In uranium nitride UN, a similar charge transfer of 1.6 electrons between U and N atoms was calculated by Kotomin *et al.*[16] with the same first-principles method.

E. Calculated properties of UC_2 and U_2C_3

Two other compounds which exist in the U-C phase diagram are studied here: the cubic U_2C_3 compound and the UC_2 compound in its tetragonal (α-UC_2) and cubic (β-UC_2) phases. These compounds appear over a large domain of compositions and coexist in some given conditions with the monocarbide UC.[3] The calculation of their structure and formation energy in the GGA approximation will give us further confidence in the use of this approximation for the study of this class of material.

The formation energies of the compounds are defined as the difference between the cohesive energies of the compound and of its constitutive elements, here the metallic α-U phase and the C graphite phase, according to the decomposition reactions as follows:

$$\alpha\text{-U} + \text{C(graphite)} \rightarrow \text{UC},$$

$$\alpha\text{-U} + 2\text{C(graphite)} \rightarrow \text{UC}_2,$$

$$2\alpha\text{-U} + 3\text{C(graphite)} \rightarrow \text{U}_2\text{C}_3,$$

which yield the following expression for the formation energies per atom:

$$E_{form}(\text{U}_p\text{C}_q) = \frac{E(\text{U}_p\text{C}_q) - pE(\alpha\text{-U}) - qE(\text{Cgraphite})}{p+q} \quad (1)$$

These expressions require the first-principles calculation of the total energies for the U-C compounds $E(\text{U}_p\text{C}_q)$, for the α-U crystal $E(\alpha\text{-U})$ and for the carbon graphite crystal E(Cgraphite). The calculated formation energies should be expected to give a good estimation of the formation enthalpies of these compounds, as it has been shown by Sedmidubsky *et al.*[36] for actinide nitrides.

The structure and formation energies of α-UC_2, β-UC_2, and U_2C_3 are calculated with a cut-off energy of 350 eV and a $8\times8\times8$ Monkhorst-Pack k-point grid, not taking into account the spin polarization. No magnetism in U_2C_3 was evidenced experimentally.[59]

1. The structure of the α-UC_2, β-UC_2, and U_2C_3 phases

α-UC_2 appears in the U-C phase diagram for temperatures higher than 1500 °C.[3] Its existence at lower temperatures is, however, still under debate.[60] Its structure is tetragonal of type CaC_2 (space group $I4/mmm$—139).[61] The unit cell contains three atoms whose positions within the cell are characterized by an internal parameter z. The β-UC_2 phase has a fluorite CaF_2 type structure (space group $Fm3m$—225)[62] and forms at higher temperature than the α phase, above 1800 °C.[3] The U_2C_3 phase has a cubic structure of the type Pu_2C_3 (space group $I43d$—220).[63] This phase can form at temperatures up to 1800 °C.[3] The positions of the eight uranium atoms in the unit cell are characterized by an internal parameter x_1 and the positions of the twelve carbon atoms by the parameter x_2.

The results obtained for the structural properties are reported in Table III and compared to experimental data.[54,64–67]

TABLE IV. Calculated formation energies E_{form} (eV/atom) of U-C compounds and comparison to the experimental enthalpies of formation $\Delta_f H^o_{298}$ (eV/atom) (Refs. 3 and 35).

U-C	E_{form} (eV/atom)	$\Delta_f H^o_{298}$ (eV/atom)
UC B1	−0.13	−0.51,[b] −0.36 to −0.50 [a]
UC B2	+0.28	
UC B3	+0.42	
α-UC_2	−0.11	−0.29,[b] −0.19 to −0.35 [a]
β-UC_2	+0.53	
U_2C_3	−0.11	−0.38,[b] −0.38 to −0.43 [a]

[a]Reference 3.
[b]Reference 35.

The calculated structure of α-UC_2, β-UC_2, and U_2C_3 all perfectly reproduce the experimental data, with differences of 1% at most on the structural parameters a, z, x_1, and x_2. The calculation of the bulk modulus of U_2C_3 gives a first estimate of this quantity since no experimental data could be found. The value obtained of 189 GPa is close to the one calculated for UC (185 GPa). One can already conclude that the GGA-PBE approximation succeeds in perfectly reproducing the structural properties of the four uranium carbides UC, α-UC_2, β-UC_2, and U_2C_3.

2. Calculated formation energies of U-C compounds

The formation energies of the U-C compounds are discussed here, namely, UC, α-UC_2, β-UC_2, and U_2C_3. The monocarbide UC is not only considered in its equilibrium rock-salt structure (also named B1) but also in two other fictitious phases: the CsCl-type structure (B2) and the ZnS-type structure (B3). The B2 and B3 phases do not appear in the U-C phase diagram but the calculated data can be useful to refine the adjustment of empirical potentials for classical molecular-dynamics simulations on UC.[46]

The calculated formation energies for UC, α-UC_2, β-UC_2, and U_2C_3 are reported in Table IV and compared to experimental data available for the enthalpies of formation of these compounds. It is to be recalled that the formation energies calculated here do not take into account the temperature. They can only give insight into the stability of the compounds at low temperatures. The review by Matzke[35] gives the commonly accepted experimental data and the article by Chevalier and Fischer[3] shows that there exists a wide disparity in the experimental data. The formation energies are calculated here with the equilibrium crystal structure reported in the previous section for the UC(B1), α-UC_2, β-UC_2, and U_2C_3 compounds. The calculated equilibrium lattice parameter obtained for the cubic UC(B2) and UC(B3) phases are 2.966 and 5.304 Å, respectively.

Table IV shows that the monocarbide UC in the B1 structure is, as expected, the most stable compound. The UC compounds in the B2 and B3 phases have positive formation energies, reflecting the fact that they do not favorably form. The β-UC_2 phase has also a positive calculated formation energy, in agreement with the phase diagram which predicts its stability at high temperatures only. As to the α-UC_2 compound, a negative formation energy is obtained, identical to the formation energy of U_2C_3. The calculations here thus suggest that the α-UC_2 phase could be thermodynamically stable at low temperature. Recent experiments showed that the α-UC_2 phase could indeed be synthesized at low temperatures,[60] but this is still in contradiction with the phase diagram of UC (Ref. 3) and recent thermodynamic calculations using the CALPHAD method.[68] It is, however, to be stressed that the thermodynamic calculations predict that the α-UC_2 compound only exists with a deficiency of carbon atoms, that is with a composition $UC_{1.9}$. This deviation from stoichiometry is not taken into account in the first-principles calculations here.

TABLE V. Calculated formation energies E_{form} (eV/atom) for nonstoichiometric UC compounds.

U-C	E_{form} (eV/atom)
UC	−0.13
$UC_{0.969}$	−0.12
$UC_{0.938}$	−0.11

Table IV shows that the overall agreement between the calculated formation energies and the experimental enthalpies of formation is not very good, in contrast to what could be found for uranium nitride.[36] It should be investigated in the future if the use of the GGA+U approximation for the modeling of these carbide phases would not bring the calculated and the experimental values to a better agreement.

Finally, using Eq. (1) the formation energies are also calculated for the B1 monocarbide UC as a function of the deviation from stoichiometry. The calculations are performed in the same conditions as those used for the bulk modulus and described in the previous section, with a 64-atom supercell containing one or two carbon vacancies. The results are given in Table V and show that the stoichiometric UC compound is more stable than the hypostoichiometric $UC_{0.969}$ and $UC_{0.938}$ ones.

IV. POINT DEFECTS IN URANIUM CARBIDE

The previous study of U-C bulk compounds gave insight into the ability of the DFT-GGA approach to model uranium carbides. We may now turn to the study of point defects and impurities in the uranium monocarbide UC. The point defects as follows are explicitly taken into account in the calculations: uranium and carbon vacancies, uranium and carbon interstitials at the tetrahedral site, uranium and carbon dumbbells (i.e., interstitial pairs around a vacant crystal site), antisite defect (exchange of neighboring uranium and carbon atoms), uranium-carbon, uranium-uranium, and carbon-carbon bivacancies, uranium and carbon Frenkel pairs (one vacancy and one interstitial of the same chemical type).

For each type of defects, the formation energy is calculated and the perturbation induced on the crystal, i.e., the atomic arrangement around the defects and the charge transfer, is analyzed. In the case of complex defects (Frenkel

TABLE VI. Calculated bulk properties of metallic α uranium: lattice parameters a (in Å), b/a, and c/a, internal structural parameter y and bulk modulus B (in GPa). Those results are compared to experimental data (Ref. 70).

U-α	a (Å)	b/a	c/a	y	B (GPa)
Calc.	2.80	2.09	1.76	0.10	152
Expt. (Ref. 70)	2.84	2.06	1.74	0.10	104

pairs, bivacancies,…) the interaction between the single point defects is also assessed.

A. Calculation of the formation energy of point defects

The first-principles PAW method allows us to consider UC supercells containing up to hundred atoms and thus to carefully check the convergence of the defect formation energies as a function of the supercell size. Indeed, in too small a supercell and because of the periodic boundary conditions, a point defect interacts with its image in the adjacent supercell, which yields a spurious contribution to the calculated formation energy. To check this convergence, we have considered supercells representing repetition of the elementary eight-atom cubic cell according to the following repetition pattern: $2\times1\times1$ (16 atoms), $2\times2\times1$ (32 atoms), $2\times2\times2$ (64 atoms), and $3\times2\times2$ (96 atoms). The defect-formation energies are then calculated with the expressions as follows:

Formation energy of a vacancy E_F^{VacX}

$$E_F^{VacX} = E_{\mathrm{UC}}^{VacX} - E_{\mathrm{UC}} + E_X. \tag{2}$$

Formation energy of a bivacancy $E_F^{BiVacXX'}$

$$E_F^{BiVacXX'} = E_{\mathrm{UC}}^{BiVacXX'} - E_{\mathrm{UC}} + E_X + E_{X'}. \tag{3}$$

Formation energy of an interstitial (tetrahedral or dumbbell) E_F^{IntX}

$$E_F^{IntX} = E_{\mathrm{UC}}^{IntX} - E_{\mathrm{UC}} - E_X. \tag{4}$$

Formation energy of a bound Frenkel pair E_F^{FPX}

$$E_F^{FPX} = E_{\mathrm{UC}}^{FPX} - E_{\mathrm{UC}}. \tag{5}$$

Formation energy of an antisite defect E_F^{AS}

$$E_F^{AS} = E_{\mathrm{UC}}^{AS} - E_{\mathrm{UC}}, \tag{6}$$

where E_{UC} is the energy of the defect-free UC supercell, E_{UC}^{VacX}, E_{UC}^{IntX}, $E_{\mathrm{UC}}^{BiVacXX'}$, E_{UC}^{FPX}, and E_{UC}^{AS} are the energies of the supercell containing one type of defect (vacancy, interstitial, bivacancy, Frenkel pair, and antisite defect, respectively). E_X is the energy per atom of each chemical species in its reference state (X=U or C). Here the reference states are chosen as the ground-state crystalline phases of uranium and carbon, namely, the α-uranium crystal and the carbon graphite phase. The calculated bulk properties of these two crystals are discussed thereafter.

The formation energies of bound Frenkel pairs [Eq. (5)] are calculated with an interstitial and a vacancy in the same supercell. They can be compared to the formation energies of *isolated* Frenkel pairs E_F^{FPXi}, that is with the interstitial and the vacancy far enough not to interact, and which can thus be determined from the formation energies of the vacancy and of the interstitial calculated separately

$$E_F^{FPXi} = E_F^{VacX} + E_F^{IntX}. \tag{7}$$

As seen in the above expressions (2)–(4), the determination of the formation energies of vacancies and interstitials requires the knowledge of an arbitrary reference energy E_X taken here as the one of a carbon and a uranium atom in their solid phase. Table VI and VII, respectively, give the bulk properties calculated for α uranium and for graphite and diamond carbon in the GGA-PBE approximation. The comparison with experimental data is good, except for the c/a ratio of the carbon graphite phase. This comes as no surprise since the interactions between carbon layers are of van der Waals type, which are not well described in the DFT/GGA. The energy difference calculated between the carbon graphite phase and the carbon diamond phase (−0.13 eV/atom) is,

TABLE VII. Calculated bulk properties of carbon in the diamond and the graphite phases, and comparison to calculations with the all-electron FLAPW method and with experimental data: lattice parameters a (in Å) and c/a, bulk modulus (in GPa), and relative stability ΔE (in eV/atom) between the two carbon phases.

C		a (Å)	c/a	B (GPa)	ΔE (eV)
Diamond	Calc.	3.577	1	432	
	Calc.[a]	3.572	1	433	
	Expt.	3.568	1	446	
Graphite	Calc.	2.472	1.638		−0.13
	Calc.[a]			25	−0.14
	Expt.	2.462	1.363	34	<0

[a]Reference 69.

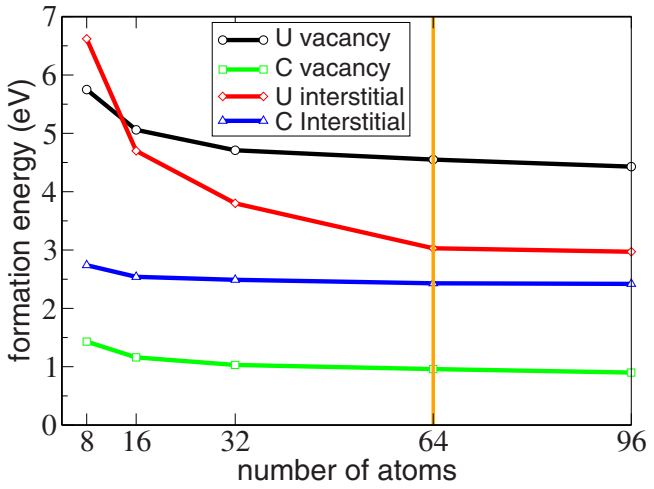

FIG. 4. (Color online) Formation energies of single point defects (vacancies and tetrahedral interstitials) in UC as a function of the size of the supercell used in the calculation.

however, small and the agreement with the more accurate FLAPW method is very good.[69] It gives an indication that the error committed on the energy of the carbon graphite phase should hardly exceed 0.1 eV/atom and will thus not be significant in the formation energies calculated according to this reference state. Concerning the α-uranium phase, the discrepancy on the calculated bulk modulus (152 GPa against 104 GPa in a recent experiment[70]) can be attributed to the neglect in our calculations of the anisotropic compression features of this metal.[71]

Figure 4 represents the variation in the calculated formation energies of the single point defects (vacancies and tetrahedral interstitials) as a function of the size of the supercell, in particular for supercells containing 8, 16, 32, 64, and 96 atoms. For a 64-atom supercell one sees that the formation energies are already well converged by comparison with the results for a 96-atom supercell. The defects whose formation energies converge the slowest are the uranium vacancies. The difference in formation energy using a 64- and 96-atom supercell is 0.1 eV at most for uranium vacancies. In the rest of the paper, all the results reported are obtained with a 64-atom supercell.

In the following sections, the stability of the different types of defects investigated is discussed. First the elementary single point defects: vacancies and interstitials at the tetrahedral site, and then the more complex defects constituted of several atoms or several single defects (dumbbells, bivacancies, etc.).

B. Single point defects: Vacancies and interstitials

Table VIII gives the formation energies of carbon and uranium vacancies, tetrahedral interstitials and isolated Frenkel pairs, all of which are calculated with a 64-atom supercell taking into account atom relaxation, and with or without volume relaxation. The variation in the lattice parameter $\Delta a/a$ of the supercell is also reported. This variation is only indicative of the degree of convergence of the size of the supercell: ideally, for an infinite-size supercell, this variation should be zero. It is also to be stressed that the interstitials here occupy tetrahedral sites, i.e., the center of a U-C simple cube. We will see in the next section that interstitials also exist in dumbbell configurations.

In Table VIII one sees that the carbon defects have lower formation energies than uranium defects. Radiation damage and deviation from stoichiometry will thus be preferably accommodated in the carbon sublattice: by the formation of carbon vacancies in hypostoichiometric UC and by the formation of carbon interstitials in hyperstoichiometric UC, for instance.

The effect of volume relaxation on the formation energies is at most 0.1 eV, except for the uranium interstitial for which it is 0.3 eV. For this latter defect, the supercell size variation is the largest, but does not, however, exceed 1%.

Few experimental data exist on the point-defect formation energies in UC. For carbon vacancies, the calculated formation energies and the experimental data are in good agreement. By electric conductivity measurements, Schüle and Spindler[31] report a carbon vacancy-formation energy of 1.0 ± 0.1 eV, and Matsui *et al.* a value of 0.8 ± 0.1 eV for UC polycrystals,[33] refined later to 1.1 ± 0.3 eV for single crystals.[34] The experimental energy for the carbon Frenkel pair is an estimate from thermodynamic data[29] and appears slightly underestimated compared to our calculated value.

As for the uranium defects, experimental data only exist for uranium vacancies and they span a wide range of values: between 1.4 and 1.7 eV for Schüle and Spindler,[31] 1.7 eV for Donner and Schüle,[30] and estimated to be 1.55 eV by Matsui and Matzke[33] and re-evaluated to 3.7 eV[34] by Matsui *et al.*

TABLE VIII. Formation energies E_F (in eV) of point defects in UC: uranium and carbon vacancies (Vac), tetrahedral interstitials (Int), and isolated Frenkel pairs (FPi). The energies are calculated with atom relaxation (pos) and with atom and volume relaxation (pos+vol), and compared to data calculated with empirical potentials (Ref. 46) and to experimental data (Refs. 29–31 and 33–35). $\Delta a/a$ is the variation in the lattice parameter of the 64-atom supercell.

E_F	Vac U	Vac C	Int U	Int C	FPi U	FPi C
E_F (eV) pos	4.55	0.83	3.03	2.56	7.58	3.39
E_F (eV) pos+vol	4.54	0.80	2.74	2.51	7.28	3.31
Empirical potentials (Ref. 46)					6.8	1.5
Experiments (Refs. 29–31 and 33–35)	1.4–3.7	0.8–1.1				2.2
$\Delta a/a$	−0.1%	−0.3%	+0.8%	+0.3%		

for single crystals. The largest experimental value of 3.7 eV is considered by Matzke[35] as the most reliable one and happens to be the closest to our calculated value of 4.5 eV.

The overall comparison with experimental data is, however, difficult, since few experimental data are available. It is also to be stressed that the calculated formation energies of vacancies and interstitials require an arbitrary reference energy [see Eqs. (2)–(4)], which we chose as the energy of the elements in their pure solid phase. Had the energy of the elements as isolated atoms been chosen, the formation energy of vacancies would be shifted by +7 eV for carbon and by +5 eV for uranium vacancies (and, respectively, by −7 and −5 eV for interstitials). With such references, the calculated formation energies would be in strong disagreement with the experimental values. Even if the choice is somewhat arbitrary, the pure solid phases as references appear more appropriate.

An analysis of the perturbation of the crystal structure induced by the different types of defects reveals the following interesting features. The carbon vacancy almost induces no perturbation of the crystal: the displacements of the six uranium first-nearest-neighbor (1nn) atoms are on the order of 0.05 Å toward the vacancy. The carbon vacancies induce thus a small *inward* relaxation of the neighboring atoms.

The uranium vacancy induces a larger relaxation of the neighboring carbon atoms, of 0.20 Å. The relaxation is here *outward*: the uranium vacancy repels the 1nn carbon atoms. In other carbides and nitrides in the rock-salt structure, such an outward relaxation of the surrounding atoms in presence of vacancies could also be evidenced in ZrC (Ref. 72), UN,[16] TiN, ZrN, and HfN.[44] In UC, the uranium and carbon atoms which are in the second coordination shell are almost not affected by the presence of the vacancy, with displacements of at most 0.05 Å for the twelve second-nearest-neighbor (2nn) uranium atoms.

The carbon tetrahedral interstitials cause an outward relaxation of the four carbon 1nn atoms of 0.22 Å, in contrast to the four uranium 1nn atoms which are almost not affected and displaced of only 0.06 Å. The displacements of the carbon and uranium 2nn atoms are again negligible, at most 0.03 Å.

The uranium tetrahedral interstitials induce the largest perturbation of all single defects investigated. They cause a displacement of 0.41 Å of the surrounding uranium atoms and of 0.16 Å of the carbon atoms. These defects are also the only ones that substantially affect the second-nearest-neighbor shell, with displacements of 0.16 Å of the carbon atoms, but negligible ones for uranium.

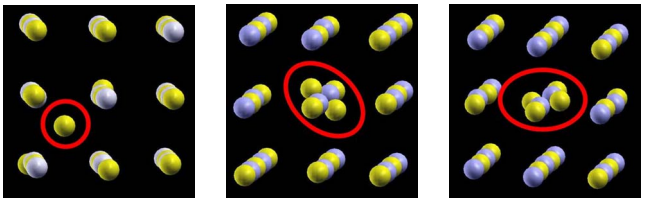

FIG. 5. (Color online) Carbon interstitials: at a tetrahedral site (left), in a dumbbell along the ⟨111⟩ direction (middle) and a dumbbell along the ⟨110⟩ direction (right). The carbon atoms are in yellow, the uranium ones in blue.

In summary, single defects such as vacancies and interstitials perturb only very little the crystalline structure of UC. Small displacements of atoms of not more than 0.4 Å appear in the immediate vicinity of the defects and hardly affects the lattice beyond the first-nearest-neighbor shell or beyond the second-nearest-neighbor shell if uranium interstitials are involved. This weak perturbation is also indicated by the small volume variation of the 64-atom supercell induced by the presence of the defects.

Preliminary calculations on the migration of single point defects in UC, using the nudge elastic band method,[73] show that U and C vacancies display an identical migration energy of 2.2 eV. It is interesting to note that in the other metallic rock-salt uranium compound UN, and using the same calculation method, Kotomin *et al.*[37] found U and N vacancies to have identical migration energies as well. Migration mechanisms of point defects in UC will be further investigated in a future study.

C. Carbon and uranium dumbbells

In the previous section, interstitial atoms were localized at the tetrahedral site. But in many carbides or nitrides, interstitials in dumbbell configurations can also be found. The stability of such defects in UC is investigated here. The stability of dumbbells oriented along different crystallographic directions is assessed: along the ⟨110⟩ direction (i.e., along the diagonal of the face of the cube) and along the ⟨111⟩ direction (i.e., along the cube diagonal). The stability of dumbbells is investigated in both the carbon and the uranium sublattice. Carbon interstitials in their different configurations are sketched on Fig. 5. The formation energies of the dumbbells [calculated according to Eq. (4)] are given in Table IX. In this table the formation energies of interstitials at the tetrahedral site are also recalled.

TABLE IX. Formation energies (in eV) with volume and atom relaxation of the C_2 and U_2 dumbbells in the ⟨111⟩ and the ⟨110⟩ orientations and of the tetrahedral interstitials (tetra), binding distances d (in Å) of the dumbbells and average charge transfer ΔQ on the interstitial atoms (in number of electrons, relative to the perfect crystal).

	C_2 ⟨111⟩	C_2 ⟨110⟩	C tetra	U_2 ⟨111⟩	U_2 ⟨110⟩	U tetra
E_F (eV)	2.18	2.16	2.51	2.18	5.06	2.74
d (Å)	1.41	1.39	2.19	2.59	2.40	2.55
ΔQ (e^-)	−0.5	−0.5	−0.3	+1.0	+0.9	+0.9

Carbon interstitials as dumbbells are found more stable than carbon interstitials at the tetrahedral site. And among the two different types of dumbbells considered, those oriented along the ⟨110⟩ direction have a slightly lower formation energy than those oriented in the ⟨111⟩ direction. The difference in energy is, however, found so small, only 0.02 eV, that dumbbells in both orientations could coexist.

The stability of carbon dumbbells in UC is in agreement with the experiments by Sarian,[28] who shows the existence of such C_2 complex centered at a carbon lattice site. The author also stresses the importance of such dumbbells in the migration mechanism of carbon interstitials. Using neutron diffraction, Bowman *et al.*[27] have also evidenced the presence of C_2 groups in the UC structure. The authors suggest, moreover, that these complexes are either freely rotating or oriented along the ⟨111⟩ direction. The small difference in the formation energies calculated here for the two types of dumbbells suggests that dumbbells coexist in the two orientations or could be indeed freely rotating. Furthermore, the calculated distance between the two carbon atoms forming the dumbbells is in good agreement with the distances experimentally determined: from 1.32 to 1.40 Å for Bowman *et al.*[27] versus our calculated values of 1.39 and 1.41 Å in Table IX.

For comparison with UN, the first-principles calculations by Kotomin *et al.*[37,38] show that N dumbbells are less stable than tetrahedral interstitials, contrary to what is found in UC. And in transition-metal nitrides, calculations give N dumbbells along the ⟨110⟩ direction more stable in TiN, but not in ZrN and HfN in which tetrahedral interstitials are energetically more favorable.[44] In the ionic-oxide MgO, which has also the rock-salt structure, oxygen interstitials are also more stable as ⟨111⟩ dumbbells.[42]

Uranium dumbbells are also found stable in UC. In Table IX the formation energies of uranium dumbbells oriented along the ⟨110⟩ and the ⟨111⟩ directions are compared to those of the uranium interstitial at the tetrahedral site. Contrary to carbon dumbbells, the orientation of the uranium dumbbells is found to have a significant importance: the ⟨111⟩ dumbbell is much more stable than the ⟨110⟩ dumbbell, with an energy difference of approximately 3 eV. And a uranium interstitial is more stable as a ⟨111⟩ dumbbell than as a tetrahedral interstitial with an energy difference of 0.56 eV. Experimentally, no publication refers to the existence of such uranium dumbbells. But in other compounds, such as transition-metal nitrides, dumbbells of metal atoms were also predicted by first-principles calculations: metal-atom dumbbells should exist in TiN, ZrN, and HfN.[44] These dumbbells are found more stable than the tetrahedral interstitials for TiN (by 0.16 eV), for ZrN (by 0.82 eV), and for HfN (by 1.56 eV). The most stable dumbbells are oriented in the ⟨111⟩ direction for TiN and ZrN (like in UC) and in the ⟨110⟩ direction for HfN.

In ZrC, the analysis of point defects induced by collision cascades simulated using classical molecular dynamics shows that carbon defects consists in majority of vacancies or interstitials, and that these interstitials are either isolated at tetrahedral sites or form dumbbells in the ⟨111⟩ direction.[40] As for zirconium defects, vacancies and ⟨111⟩ Zr dumbbells could be found, but no isolated interstitials. One can predict a similar behavior for the defect formation in UC after collision cascades, in the light of the formation energies of defects calculated here.

The partial charge transfer ΔQ on the interstitial atoms at a tetrahedral site or as dumbbells, relative to the charge of U and C atoms in defect-free UC, are given in Table IX. It shows that carbon dumbbells are stabilized by a larger charge transfer compared to the isolated tetrahedral interstitial. The two carbon atoms forming the dumbbell lose around 0.2 more electrons than the tetrahedral interstitial, i.e., they lose 0.5 electrons compared to C atoms in defect-free UC. Both types of dumbbells, in the ⟨110⟩ and the ⟨111⟩ directions, induce similar perturbation of the charge density, which explains their similar formation energies. Uranium interstitials induce a larger charge transfer, they gain around 1 electron. The ⟨111⟩ dumbbell is the most stable and is also stabilized by a larger charge transfer compared to the other dumbbell and to the tetrahedral interstitial. In UN, according to the first-principles calculations by Kotomin *et al.*,[16] the situation is similar for N tetrahedral interstitials: they also lose 0.5 electrons compared to the occupation of N atoms in the UN crystal.

D. Bound Frenkel pairs

The formation energies of bound and isolated Frenkel pairs are compared here. It is first recalled that a Frenkel pair is constituted of an interstitial atom and of a vacancy of the same chemical element. If the interstitial and the vacancy are in neighboring positions in the crystal, the Frenkel pair is said to be bound. This can be modeled considering both single point defects in the same supercell. If the interstitial and the vacancy are sufficiently far away not to interact, the Frenkel pair is said to be isolated. In this case, the formation energy of the isolated Frenkel pair can be calculated as the sum of the formation energies of the interstitial and of the vacancy, calculated separately.

In the case of bound Frenkel pairs, one can chose different relative positions in the supercell for the vacancy and for the interstitial constituting the defect. If the interstitial is located at the center of the cube containing the vacancy (i.e., with a separation distance of 2.13 Å), the two single defects recombine: the Frenkel pair is not stable (for both uranium and carbon Frenkel pairs). On the other hand, if the interstitial is located in the adjacent cube (i.e., with a separation distance of at least 4.09 Å), the Frenkel pair is then stable. This configuration of the Frenkel pair is represented in Fig. 6. One can also investigate the stability of Frenkel pairs for which the interstitial is not at the tetrahedral site but forms a dumbbell. All those configurations of Frenkel pairs have been studied in the carbon and the uranium sublattices, and the corresponding formation energies for bound and isolated Frenkel pairs are compared in Table X. Note that only the most stable dumbbell configurations are taken into account: the ⟨110⟩ orientation for the carbon dumbbell and the ⟨111⟩ orientation for the uranium dumbbell.

Table X shows that Frenkel pairs are more stable with dumbbell interstitials than with tetrahedral interstitials. The difference in the formation energies is small between the

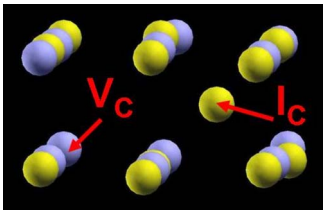

FIG. 6. (Color online) Bound carbon Frenkel pair. The carbon atoms are in yellow, the uranium atoms in blue. The positions of the vacancy and of the interstitial (Vc and Ic, respectively) are indicated by the arrows.

bound and isolated configurations, and this for both the uranium and for the carbon Frenkel pairs. In the most favorable configuration of the Frenkel pair (with a dumbbell), the binding energy is less than 50 meV for carbon and uranium. This denotes the very short-range interaction between the single point defects. Beyond the first-nearest-neighbor shell, a carbon vacancy and a carbon interstitial almost do not feel each other anymore. The recombination distance of Frenkel pairs in UC is thus also found small, and smaller than the lattice parameter: a vacancy and an interstitial are found stable when separated by more than 0.8 times the lattice parameter only. By contrast, in the ionic uranium dioxide, classical molecular dynamics studies show that the recombination radius is around 6 Å,[74] i.e., larger than the lattice parameter (5.47 Å).

It is also to be noted that, although very small, the interaction between the vacancy and the dumbbell is attractive for carbon (i.e., the bound configuration is more stable) and repulsive for uranium (i.e., the isolated configuration is more stable).

E. Bivacancies U-C, U-U, and C-C

Vacancies and bivacancies constitute potential traps for fission products, helium atoms produced by α decay or other impurities. Thus, besides the single vacancies studied in the previous section, the formation of bivacancies is also investigated. The bivacancies considered here are constituted either of two uranium vacancies or of two carbon vacancies or of one carbon and one uranium vacancy. Various configurations of those bivacancies can be considered. For the C-C and U-U bivacancies, the single vacancies occupy nearest-neighbor sites. The U-C bivacancies can be formed with U and C single vacancies that are either oriented along the ⟨100⟩ direction or along the ⟨111⟩ direction. Those two latter configurations are represented in Fig. 7. The formation energies calculated for all those bivacancies are reported in Table XI.

TABLE X. Formation energies (in eV) of bound Frenkel pairs (FP) in which the interstitial is at a tetrahedral site (tetra) or form a dumbbell (⟨110⟩ or ⟨111⟩), compared to the formation energies (in eV) of isolated Frenkel pairs. E_b (in eV) is the binding energy of the elementary defects. The formation energies reported are those obtained after volume relaxation.

	FP C tetra	FP C ⟨110⟩	FP U tetra	FP U ⟨111⟩
E_F (eV) bound	3.33	2.94	7.42	6.75
E_F (eV) isolated	3.31	2.96	7.28	6.72
E_b (eV)	+0.02	−0.02	+0.13	+0.03

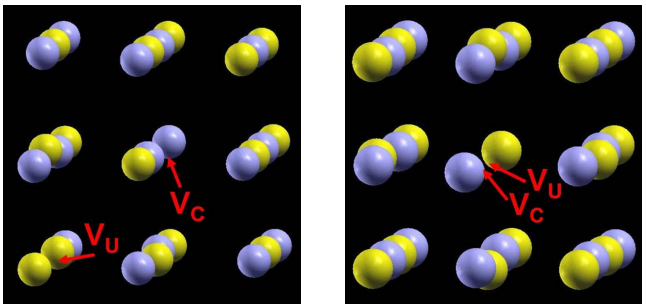

FIG. 7. (Color online) Left: U-C bivacancy oriented along the ⟨111⟩ direction. Right: U-C bivacancy oriented along the ⟨100⟩ direction. Carbon atoms are in yellow, uranium atoms in blue. The positions of the carbon and uranium single vacancies (V_C and V_U, respectively) forming the bivacancies are indicated by the red arrows.

As it can be seen in Table XI, the formation of a bivacancy containing a uranium vacancy is very unfavorable, with high formation energies of around 5 eV for U-C and U-U bivacancies. The formation of a C-C bivacancy only costs 1.85 eV.

The interaction between the two vacancies constituting the bivacancies is investigated by comparing their formation energies to the sum of the formation energy of the two isolated single vacancies. Bivacancy containing a uranium vacancy (i.e., U-C and U-U bivacancies) are attractive: their formation energies are lower by 0.8 eV when the vacancies are near and bound than when they are isolated, suggesting that clustering of such vacancies will occur. On the other hand, C-C bivacancies have a repulsive interaction. The binding energies of bivacancies are actually decreasing fast with increasing distance between the two vacancies. This can be seen in Table XI for the U-C bivacancy in its two configurations, when the vacancies are in first-nearest-neighbor positions (Bivac U-C ⟨100⟩) and in second-nearest-neighbor position (Bivac U-C ⟨111⟩). Vacancies that are separated by more than the lattice parameter distance almost do not interact.

By comparison to first-principles calculations on other compounds in the rock-salt structure, such as the transition-

TABLE XI. Formation energies (in eV) of U-C, U-U, and C-C bivacancies with atom and volume relaxation, formation energies of the corresponding isolated vacancies, binding energy E_b (in eV) of the two vacancies constituting the bivacancy.

	Bivac U-C ⟨111⟩	Bivac U-C ⟨100⟩	Bivac U-U ⟨110⟩	Bivac C-C ⟨110⟩
E_F (eV)	5.32	4.59	8.32	1.85
E_F (eV) isolated	5.34	5.34	9.08	1.60
E_b (eV)	−0.02	−0.75	−0.76	+0.25

TABLE XII. Incorporation energies (in eV) of helium, xenon, and oxygen atoms in UC at different crystal sites—uranium and carbon substitution sites (site U and site C), tetrahedral interstitial site (Int.), U-C bivacancies (bivac.)—with relaxation of the atom positions (pos) and volume of the supercell (vol), change in the supercell lattice parameter $\Delta a/a$ and effective charge Q of the incorporated atoms.

E_{inc} (eV)	Site U	Site C	Site Int.	Bivac. ⟨100⟩	Bivac. ⟨111⟩
He (pos)	0.72	2.60	3.00	0.65	0.71
He (pos+vol)	0.72	2.64	2.97	0.68	0.74
$\Delta a/a$ (%)	~0	−0.1	+0.2	−0.4	−0.4
Q(He)	−0.1	−0.1	~0	−0.1	−0.1
Xe (pos)	4.26	8.64	12.81	3.16	4.24
Xe (pos+vol)	4.19	8.22	12.09	3.22	4.31
$\Delta a/a$ (%)	+0.4	+0.9	+1.2	+0.1	+0.1
Q(Xe)	+0.1	−0.3	~0	−0.1	+0.1
O (pos)	0.54	−5.88	−2.84	−5.64	−5.85
O (pos+vol)	0.54	−5.85	−2.91	−5.57	−5.77
$\Delta a/a$ (%)	−0.1	~0	+0.3	−0.2	−0.2
Q(O)	−0.8	−1.4	−1.2	−1.3	−1.4

metal nitrides TiN, ZrN, and HfN, no clustering of N vacancies were predicted as well.[44]

F. Antisite defect

Finally, the stability of an antisite defects in UC is investigated. Such a defect consists of an exchange of a U and a C atom in the crystal, here in a 64-atom supercell. The calculated formation energy of the antisite defect in a perfect rocksalt lattice of UC without any relaxation of the atomic position amounts to 10.4 eV. It is thus very large and already suggests that such a defect is highly unstable. When the relaxation of the atomic position is allowed, the antisite defect indeed reveals to be not stable. The defect evolves toward a dumbbell-type defect. This instability can be understood considering the great difference of atomic radius and of electronegativity between uranium and carbon atoms. The calculations here thus predict that the antisite defect does not exist in UC.

V. INCORPORATION OF HELIUM, XENON, AND OXYGEN ATOMS IN UC

In this section, the stability of rare gases and oxygen impurities in the UC lattice is studied. Helium and xenon can be found in UC as a result of α decay and fission reactions and oxygen as a result of oxidation. The determination of their incorporation energies enables us to assess their stability as isolated impurities in various crystallographic sites, and thus their most favorable location in the lattice.

The incorporation energy is defined as the energy required to incorporate an atom (from infinity) at a pre-existing vacancy or at an interstitial site, according to the expression as follows:

$$E_{inc} = E_{\mathrm{UC}}^{X} - E_{\mathrm{UC}} - E_{X}, \tag{8}$$

where E_{UC}^{X} is the energy of the UC supercell with the incorporated X impurity, E_{UC} is the energy of the supercell with the vacant host site, and E_X is the energy of the isolated xenon or helium atom or of an oxygen atom in an isolated dioxygen O_2 molecule in its triplet state.

The incorporation energies are calculated in a 64-atom UC supercell for various incorporation sites: the uranium and the carbon substitution sites, the tetrahedral interstitial site and the U-C bivacancies oriented along the ⟨100⟩ and the ⟨111⟩ directions (cf. Fig. 7). The relaxation of the atomic positions in the supercell is always taken into account. The calculated incorporation energies for helium, xenon, and oxygen in UC, with and without volume relaxation, are reported in Table XII. The results given for a fixed lattice parameter and with atomic relaxation (labeled *pos*) are obtained with the calculated equilibrium lattice parameter of defect-free UC. The fully relaxed results [labeled (*pos+vol*)] are obtained after atomic relaxation and lattice parameter relaxation of the two supercells: the one containing the impurity and the one containing the vacant host site. Depending on the relaxation energy gains of those two different systems, the fully relaxed incorporation energy can be smaller or larger than the locally relaxed incorporation energy. The size variation of the supercell is indicative of the degree of perturbation induced by the impurity on the 64-atom supercell. For a given impurity, the lowest incorporation energy corresponds to the most favorable incorporation site. And a negative value of the incorporation energy means that this element is energetically stable in the crystal, compared to the impurity element in its reference state (isolated atom or molecule). Like in the case of the point defects, tests were performed in order to make sure that the incorporation energies calculated here in a 64 atom supercell were converged as a function of the size of the supercell. The variation in the 64-atom supercell size after incorporation of the impurities is discussed below, as it gives an indication as well on the degree of convergence of the supercell size.

A. Location and stability of He, Xe, and O impurities in UC

The calculated incorporation energies show that the rare-gas atoms helium and xenon are more stable in the largest traps available: in a single uranium vacancy or in the uranium vacancy of a U-C bivacancy. The incorporation energies are very close for all those types of defects, but for both helium and xenon, the incorporation energy is the lowest for the U-C bivacancy oriented in the ⟨100⟩ direction. Helium has a small incorporation energy, of around 0.7 eV, contrary to xenon whose incorporation energy is much larger, around 4.2 eV. In both cases, the incorporation energy is positive, meaning that those elements are not stable in the UC crystal. The smaller value obtained for helium could, however, rather place this element at the edge of solubility in UC. Xenon is clearly nonsoluble in UC and has probably a high propensity to form bubbles, as it was, for instance, already experimentally evidenced for this element in UO_2.[75]

The accuracy of the results presented here on the incorporation energies of rare-gas atoms in a crystal has, however, to be moderated. It has to be emphasized again that the DFT and the GGA approximation cannot accurately describe van der Waals interactions[76] which have a dominant contribution in the chemical binding involving rare-gas elements. This shortcoming is expected to be more important for helium atoms than for xenon atoms, as shown in a study of rare-gases incorporation in small molecules by Bertolus.[77] The importance of the van der Waals contribution for helium has also been stressed by Gryaznov *et al.*[78] in their first-principles study of helium incorporation in UO_2, in which they could assess this contribution using empirical potentials. The DFT results obtained here for UC are, however, assumed to give a reasonable trend for the behavior of helium and xenon atoms in the UC crystal.

Oxygen impurities in UC, contrary to rare-gas impurities, and due to their high electronegativity, are more stable at the carbon substitution site: in a single carbon vacancy or at the carbon site of a U-C bivacancy. The oxygen atom in these defects displays a significantly negative incorporation energy, around −5 to −6 eV, indicating a very high tendency for UC to oxidize. And this tendency to oxidation by incorporation of oxygen atoms at carbon sites is even strengthened by the fact that carbon vacancies are very numerous in UC, as indicated by their low formation energy of 0.8 eV, making thus many incorporation sites for oxygen atoms available. These results also corroborate the experimental findings by Eckle and Gouder.[79] Using photoemission spectroscopy to characterize UC samples in low oxygen partial-pressure environment, they show that the incorporation of oxygen atoms lead to the formation of a UO-UC solid solution, suggesting thus that oxygen atoms indeed occupy carbon site in the rock-salt lattice of UC. From Table XII one notices that the incorporation energy of oxygen is negative for tetrahedral interstitial sites as well (−2.9 eV), and only weakly positive at a uranium vacancies (0.5 eV), which stresses again the very favorable accommodation of oxygen atoms in the UC lattice.

TABLE XIII. Atomic displacements (Δd in Å) of the first-nearest-neighbor (1nn) atoms around the impurity (helium, xenon, and oxygen) in UC for the different incorporation sites: uranium and carbon substitution sites and tetrahedral interstitial site (Int.). The chemical type of the 1nn atoms is indicated in brackets.

Δd (Å)	Site U	Site C	Site Int.
Helium	+0.21 (C)	+0.04 (U)	+0.11 (C)/+0.09 (U)
Xenon	+0.33 (C)	+0.26 (U)	+0.40 (C)/+0.68 (U)
Oxygen	+0.28 (C)	+0.01 (U)	+0.28 (C)/+0.05 (U)

B. Perturbations of the UC crystal by the incorporation of He, Xe, and O atoms

In this section, the perturbations of the crystal induced by the impurities are analyzed in more detail: first the structure and then the charge density.

1. Atom displacements around the impurities

It is to be noted first that the variation in the size of the supercell induced by the incorporation of a helium, a xenon, or an oxygen atom is not very important. The volume relaxation with the incorporated elements has not a great influence on the incorporation energies (see Table XII). In their most favorable incorporation site, helium induces a slight contraction of the lattice (−0.4% in a ⟨100⟩ bivacancy and less than −0.1% at the uranium site), xenon induces a slight expansion (+0.4% at the uranium site, +0.1% in the ⟨100⟩ bivacancy) and oxygen a contraction even smaller (−0.2% in the ⟨100⟩ bivacancy and less than −0.1% at a carbon site). In those favorable configurations, the volume relaxation induces a variation in the incorporation energies of less than 0.1 eV, showing that the 64-atom supercell is big enough to get reliable results. The largest variation in the lattice parameter and of the incorporation energy is obtained for a very unfavorable incorporation site of xenon, the interstitial site, with variations of +1.2% and 0.7 eV, respectively.

Table XIII gives the displacements of the atoms in the first coordination sphere around the incorporated elements. Those displacements are determined for the three different incorporation site of each impurity: the uranium and the carbon substitution sites and the tetrahedral interstitial site. The atomic displacement Δd is defined as the displacement relative to the position of the atom in the perfect rock-salt structure of UC. It can be considered that a displacement of less then 0.05 Å, i.e., less than 1% of the UC lattice parameter, is negligible.

Helium incorporation. For the most favorable helium incorporation site (the uranium site), the six 1nn carbon atoms are repelled by +0.21 Å. Such a displacement is identical to the one obtained for a uranium vacancy (+0.20 Å, see previous section). It is thus apparently not the presence of the helium atom which is the cause of this outward relaxation of the lattice, but rather the missing uranium atom. The second coordination sphere is not affected by the presence of the helium atom, with displacements of at most 0.04 Å only.

Xenon incorporation. As expected from its larger atomic radius compared to helium, xenon induces a greater pertur-

bation of the crystal. At a uranium substitution site, the xenon atom repels the six carbon 1nn atoms by +0.33 Å, which is much larger than the displacement induced by the uranium vacancy. The 12 uranium 2nn are displaced by 0.02 Å, which is again negligible. Only the incorporation of xenon at a tetrahedral interstitial site would perturb the lattice beyond the first coordination sphere, but the location of xenon at this site is highly improbable, the incorporation energy of xenon being larger than 10 eV.

Oxygen incorporation. In its most favorable incorporation site (the carbon site), an oxygen atom does almost not perturb the crystal structure at all, with negligible displacements of even the nearest-neighbor atoms. One can also note that when incorporated at the interstitial site, the oxygen atom strongly repels the surrounding carbon atoms whereas the uranium ones are not significantly displaced.

Thus, just like in the case of point defects, the presence in UC of the impurities considered here perturbs only very weakly the crystalline structure: for the most favorable site of each impurity, only the atoms on 1nn positions are displaced by a significant distance.

2. Modification of the electron density

A Bader analysis[58] of the charge density of the system with a helium, a xenon, or an oxygen impurity in UC reveals the following features (see Table XII). The rare-gas impurities display only a weak charge transfer. At the tetrahedral interstitial position, they do not present any charge transfer, in agreement with a complete electronic shell and a neutral environment at this position. Only the xenon atom at the substitution carbon site (which is not its most favorable position) gains around 0.3 electrons, which can be associated to a polarization of its charge density. In the other positions, the transfer is limited to 0.1 electrons for both helium and xenon.

Oxygen displays a larger charge transfer. Whatever its position in the UC crystal, the oxygen impurity gains around 1 electron. The transfer is the largest, with a gain of 1.4 electrons, when the oxygen atom is located at the carbon site, which is a stable site of incorporation. This trend for oxygen was also found in UN using first-principles calculations.[80]

C. Comparison with first-principles results for UN

First-principles studies of the incorporation of helium and oxygen in UN also exist.[80,81] We compare here the incorporation energies obtained using the same calculation approach in order to find trends for the different uranium compounds investigated. Note that no first-principles study of xenon in UN exists so far. All the results reported in Table XIV were obtained using the PAW method and the GGA approximation.

Helium shows similar incorporation energies in UC and UN. In both materials the most favorable location is a uranium vacancy. The incorporation energies are of the same order of magnitude, around 0.5 eV. Helium appears thus not soluble in these uranium compounds but its low incorporation energies could place this element at the edge of solubility in UN too.

The incorporation of oxygen atoms is favorable in the carbide and the nitride,[80] as shows the negative incorporation energies calculated. Both the nitride and the carbide are highly oxidable, with oxygen incorporation energies less than −5 eV.

TABLE XIV. Incorporation energies (in eV) of helium and oxygen in UN and UC for various locations: U substitution site, C or N substitution site, tetrahedral interstitial site (Int.).

E_{inc} (eV)	Site U	Site C/N	Site Int.
He in UC (GGA)	0.7	2.6	3.0
He in UN (GGA) (Ref. 81)	0.5	2.5	
O in UC (GGA)	0.5	−5.9	−2.9
O in UN (GGA) (Ref. 80)		−9.2	−5.8

VI. CONCLUSION

The type of point defects likely to form in the uranium monocarbide UC has been studied here, using first-principle calculations, together with the stability in the lattice of impurities such as helium (formed by α decays), xenon (formed by fissions), and oxygen (introduced by oxidation).

The first step of the study shows that the approach used, the first-principles PAW method in the GGA approximation, could satisfactorily reproduce some properties of the bulk uranium carbides UC, UC_2, and U_2C_3. The study of point defects in UC shows that the carbon sublattice accommodates best the presence of defects. Carbon and uranium interstitials are more stable as dumbbells compared to isolated interstitials at the tetrahedral site, a feature common with other carbides or nitrides with same rock-salt structure. Furthermore, the interaction between single point defects is found short range, with an interaction sphere limited to the first or second neighbor shell. Carbon vacancies, which are present in large amount in hypostoichiometric UC, are not predicted to form vacancy clusters.

Helium and xenon impurities are shown to be more stable in the defects leaving more room: isolated uranium vacancies or the uranium vacancy of a U-C bivacancy. Helium has a positive but small incorporation energy in UC, as in UN, suggesting that helium is at the edge of solubility. Xenon has a much larger positive incorporation energy and is thus not soluble in UC. Oxygen, on the contrary, has a significantly negative incorporation energy making UC highly oxidable. The electron configuration of the oxygen atom favors its incorporation at the carbon site: either in an isolated carbon vacancy or in a carbon vacancy of a U-C bivacancy.

The perturbations induced on the UC crystal structure by the defects and the three types of impurities are very small: neighboring atoms are significantly displaced only in the first coordination sphere. This study will be completed in the future by the investigation of the migration mechanisms of uranium and carbon atoms or of impurities in UC, and by similar studies in the mixed carbide (U, Pu)C. The set of results obtained here for UC could also be useful in order to adjust or refine empirical potentials or input data for models at a larger scale, such as classical molecular dynamics, which could be appropriate to study atomic-diffusion mechanisms in uranium carbides.

ACKNOWLEDGMENTS

The comparison of the first-principles PAW and the APW+lo methods was enabled by the ACTINET project "Structural defects in binary and ternary uranium oxides" (Grant No. JPR-01-15) and by the collaboration with D. Lamoen of the University of Antwerp (Belgium). The work benefited from the support of the European program F-BRIDGE (Basic Research for Innovative Fuel Design for GEN IV systems, Contract No. 211690) and of the MATINEX program (Matériaux Innovants en conditions Extrêmes). J. Durinck, B. Dorado, M. Bertolus, R. Ducher, A. Chartier, D. Gryaznov, E. Kotomin, C. Guéneau, J. C. Dumas, and O. Tougait are acknowledged for fruitful discussions and for sharing their work prior to publication.

*michel.freyss@cea.fr

[1] D. Petti, D. Crawford, and N. Chauvin, MRS Bull. **34**, 40 (2009).
[2] D. C. Crawford, D. L. Porter, and S. L. Hayes, J. Nucl. Mater. **371**, 202 (2007).
[3] P. Y. Chevalier and E. Fischer, J. Nucl. Mater. **288**, 100 (2001).
[4] P. E. Blöchl, Phys. Rev. B **50**, 17953 (1994).
[5] G. Kresse and D. Joubert, Phys. Rev. B **59**, 1758 (1999).
[6] P. Hohenberg and W. Kohn, Phys. Rev. **136**, B864 (1964).
[7] W. Kohn and L. Sham, Phys. Rev. **140**, A1133 (1965).
[8] M. Freyss, T. Petit, and J.-P. Crocombette, J. Nucl. Mater. **347**, 44 (2005).
[9] H. Y. Geng, Y. Chen, Y. Kaneta, M. Iwasawa, T. Ohnuma, and M. Kinoshita, Phys. Rev. B **77**, 104120 (2008).
[10] D. A. Andersson, J. Lezama, B. P. Uberuaga, C. Deo, and S. D. Conradson, Phys. Rev. B **79**, 024110 (2009).
[11] G. Brillant and A. Pasturel, Phys. Rev. B **77**, 184110 (2008).
[12] B. Dorado, B. Amadon, M. Freyss, and M. Bertolus, Phys. Rev. B **79**, 235125 (2009).
[13] P. Söderlind, Phys. Rev. B **66**, 085113 (2002).
[14] C. D. Taylor, Phys. Rev. B **77**, 094119 (2008).
[15] R. Atta-Fynn and A. K. Ray, Phys. Rev. B **76**, 115101 (2007).
[16] E. A. Kotomin, Y. A. Mastrikov, Y. F. Zhukovskii, and P. van Uffelen, Phys. Status Solidi C **4**, 1193 (2007).
[17] L. Petit, A. Svane, Z. Szotek, W. M. Temmerman, and G. M. Stocks, Phys. Rev. B **80**, 045124 (2009).
[18] C.-C. Fu and F. Willaime, Phys. Rev. B **72**, 064117 (2005).
[19] M. Dion, H. Rydberg, E. Schröder, D. C. Langreth, and B. I. Lundqvist, Phys. Rev. Lett. **92**, 246401 (2004).
[20] O. A. Vydrov and T. Van Voorhis, Phys. Rev. Lett. **103**, 063004 (2009).
[21] P. Weinberger, R. Podloucky, C. P. Mallet, and A. Neckel, J. Phys. C **12**, 801 (1979).
[22] K. Schwarz and P. Herzig, J. Phys. C **12**, 2277 (1979).
[23] C. P. Mallett, J. Phys. C **15**, 6361 (1982).
[24] M. S. S. Brooks, J. Phys. F: Met. Phys. **14**, 639 (1984).
[25] J. Trygg, J. M. Wills, M. S. S. Brooks, B. Johansson, and O. Eriksson, Phys. Rev. B **52**, 2496 (1995).
[26] N. Vigier, C. D. Auwer, C. Fillaux, A. Maslennikov, H. Noel, J. Roques, D. Shuh, E. Simoni, T. Tyliszczak, and P. Moisy, Chem. Mater. **20**, 3199 (2008).
[27] A. L. Bowman, G. P. Arnold, W. G. Witteman, T. C. Wallace, and N. G. Nereson, Acta Crystallogr. **21**, 670 (1966).
[28] S. Sarian, J. Nucl. Mater. **49**, 291 (1974).
[29] Hj. Matzke, Solid State Ionics **12**, 25 (1984).
[30] D. Donner and W. Schüle, J. Nucl. Mater. **45**, 293 (1973).
[31] W. Schüle and P. Spindler, J. Nucl. Mater. **32**, 20 (1969).
[32] L. B. Griffiths, Philos. Mag. **7**, 827 (1962).
[33] H. Matsui and Hj. Matzke, J. Nucl. Mater. **89**, 41 (1980).
[34] H. Matsui, T. Kato, K. Yagi, S. Okitsu, and M. Horiki, Radiat. Eff. Defects Solids **108**, 115 (1989).
[35] Hj. Matzke, *Science of Advanced LMFBR Fuels* (North-Holland, Amsterdam, 1986).
[36] D. Sedmidubsky, R. Konings, and P. Novak, J. Nucl. Mater. **344**, 40 (2005).
[37] E. A. Kotomin, Y. A. Mastrikov, S. N. Rashkeev, and P. V. Uffelen, J. Nucl. Mater. **393**, 292 (2009).
[38] E. A. Kotomin, D. Gryaznov, R. W. Grimes, D. Parfitt, Y. F. Zhukovskii, Y. A. Mastrikov, P. van Uffelen, V. V. Rondinella, and R. J. M. Konings, Nucl. Instrum. Methods Phys. Res. B **266**, 2671 (2008).
[39] E. A. Kotomin, R. W. Grimes, Y. A. Mastrikov, and N. J. Aschley, J. Phys.: Condens. Matter **19**, 106208 (2007).
[40] L. van Brutzel and J. P. Crocombette, Nucl. Instrum. Methods Phys. Res. B **255**, 141 (2007).
[41] H. W. Hugosson, P. Korzhavyi, U. Jansson, B. Johansson, and O. Eriksson, Phys. Rev. B **63**, 165116 (2001).
[42] T. Brudevoll, E. A. Kotomin, and N. E. Christensen, Phys. Rev. B **53**, 7731 (1996).
[43] E. A. Kotomin and A. I. Popov, Nucl. Instrum. Methods Phys. Res. B **141**, 1 (1998).
[44] L. Tsetseris, N. Kalfagiannis, S. Logothetidis, and S. T. Pantelides, Phys. Rev. B **76**, 224107 (2007).
[45] L. Tsetseris, N. Kalfagiannis, S. Logothetidis, and S. T. Pantelides, Phys. Rev. Lett. **99**, 125503 (2007).
[46] A. Chartier and L. van Brutzel, Nucl. Instrum. Methods Phys. Res. B **255**, 146 (2007).
[47] http://cms.mpi.univie.ac.at/vasp/
[48] J. Hafner, J. Comput. Chem. **29**, 2044 (2008).
[49] J. P. Perdew, K. Burke, and M. Ernzerhof, Phys. Rev. Lett. **77**, 3865 (1996).
[50] H. J. Monkhorst and J. D. Pack, Phys. Rev. B **13**, 5188 (1976).
[51] G. K. H. Madsen, P. Blaha, K. Schwarz, E. Sjöstedt, and L. Nordström, Phys. Rev. B **64**, 195134 (2001).
[52] http://www.wien2k.at
[53] J. L. Routbort and R. N. Singh, J. Nucl. Mater. **58**, 78 (1975).
[54] A. E. Austin, Acta Crystallogr. **12**, 159 (1959).
[55] M. Idiri, T. LeBihan, S. Heathman, and J. Rebizant, Phys. Rev. B **70**, 014113 (2004).
[56] M. B. Brodsky, Rep. Prog. Phys. **41**, 1547 (1978).
[57] H. H. Hill, in *Plutonium and Other Actinides*, Proceedings of the Fourth International Conference on Plutonium and other Actinides, Nuclear Metallurgy Vol. 17 (AIME, New York, 1970).
[58] G. Henkelman, A. Arnaldsson, and H. Jonsson, Comput. Mater.

Sci. **36**, 354 (2006).
[59] J. L. Boutard and C. H. de Novion, Solid State Commun. **14**, 181 (1974).
[60] C. Guéneau, O. Tougait, and D. Manara (private communication).
[61] http://cst-www.nrl.navy.mil/lattice/struk/c11_b.html
[62] http://cst-www.nrl.navy.mil/lattice/struk/c1.html
[63] http://cst-www.nrl.navy.mil/lattice/struk/d5_c.html
[64] D. W. Jones, I. J. McColm, R. Steadman, and J. Yerkess, J. Solid State Chem. **68**, 219 (1987).
[65] Hj. Matzke, Solid State Commun. **12**, 401 (1973).
[66] R. C. Chang, Acta Crystallogr. **14**, 1097 (1961).
[67] J. L. Green, G. P. Arnold, J. A. Leary, and N. G. Nereson, J. Nucl. Mater. **34**, 281 (1970).
[68] C. A. Utton, F. D. Bruycker, K. Boboridis, R. Jardin, H. Noel, C. Guéneau, and D. Manara, J. Nucl. Mater. **385**, 443 (2009).
[69] J. V. Badding and T. J. Scheidemantel, Solid State Commun. **122**, 473 (2002).
[70] T. LeBihan, S. Heathman, M. Idiri, G. H. Lander, J. M. Wills, A. C. Lawson, and A. Lindbaum, Phys. Rev. B **67**, 134102 (2003).
[71] K. M. Hope, Y. K. Vohra, and T. LeBihan, High Press. Res. **25**, 235 (2005).
[72] J. Li, D. Liao, S. Yip, R. Najafabadi, and L. Ecker, J. Appl. Phys. **93**, 9072 (2003).
[73] G. Henkelman, B. P. Uberuaga, and H. Jonsson, J. Chem. Phys. **113**, 9901 (2000).
[74] L. Van Brutzel, A. Chartier, and J. P. Crocombette, Phys. Rev. B **78**, 024111 (2008).
[75] P. Garcia, P. Martin, G. Carlot, E. Castelier, M. Ripert, C. Sabathier, C. Valot, F. D'acapito, J.-L. Hazemann, O. Proux, and V. Nassif, J. Nucl. Mater. **352**, 136 (2006).
[76] F. O. Kannemann and A. D. Becke, J. Chem. Theory Comput. **5**, 719 (2009).
[77] M. Bertolus, Seventh International Workshop on Materials Models and Simulations for Nuclear Fuels (MMSNF-7), 29–30 September, Karlsruhe, Germany, 2008 (unpublished).
[78] D. Gryaznov, E. Heifets, and E. Kotomin, Phys. Chem. Chem. Phys. **11**, 7241 (2009).
[79] M. Eckle and T. Gouder, J. Alloys Compd. **374**, 261 (2004).
[80] E. A. Kotomin and Y. A. Mastrikov, J. Nucl. Mater. **377**, 492 (2008).
[81] D. Gryaznov, Seventh International Workshop on Materials Models and Simulations for Nuclear Fuels (MMSNF-7), 29–30 September, Karlsruhe, Germany, 2008 (unpublished).